Monthly Notices
of the
ROYAL ASTRONOMICAL SOCIETY

MNRAS **434,** 3463–3468 (2013)
Advance Access publication 2013 August 14

doi:10.1093/mnras/stt1259

Long-term X-ray emission from Swift J1644+57

Y. C. Zou,[1,2]★ F. Y. Wang[1,3,4]★ and K. S. Cheng[1]★

[1]*Department of Physics, University of Hong Kong, Pokfulam Road, Hong Kong, China*
[2]*School of Physics, Huazhong University of Science and Technology, Wuhan 430074, China*
[3]*School of Astronomy and Space Science, Nanjing University, Nanjing 210093, China*
[4]*Key Laboratory of Modern Astronomy and Astrophysics (Nanjing University), Ministry of Education, Nanjing 210093, China*

Accepted 2013 July 9. Received 2013 July 9; in original form 2013 February 22

ABSTRACT

The X-ray emission from Swift J1644+57 is not steadily decreasing; instead, it shows multiple pulses with declining amplitudes. We model the pulses as reverse shocks from collisions between the late ejected shells and the externally shocked material, which is decelerated while sweeping the ambient medium. The peak of each pulse is taken as the maximum emission of each reverse shock. With a proper set of parameters, the envelope of peaks in the light curve as well as the spectrum can be modelled well.

Key words: radiation mechanisms: non-thermal – X-rays: general.

1 INTRODUCTION

There have been many investigations of the tidal disruption of a star by a supermassive black hole in a galactic nucleus (e.g. Hills 1975; Lacy, Townes & Hollenbach 1982). When a star's trajectory happens to be sufficiently close to a supermassive black hole, the star will be captured and eventually tidally disrupted. After the star is disrupted, at least half of the debris is ejected from the system; the rest remains bound to the black hole and is accreted (Rees 1988; Ayal, Livio & Piran 2000). It has been predicted that the accretion of this stellar debris could power a luminous electromagnetic flare that would be expected to peak in the optical, ultraviolet (UV) and X-ray wavelengths, lasting for months to years (Ulmer 1999; Strubbe & Quataert 2009, 2011).

Swift J164449.3+573451 (also first known as GRB 110328A; hereafter Swift J1644+57) has been proposed as a tidal disruption candidate (Bloom et al. 2011; Burrows et al. 2011; Levan et al. 2011; Zauderer et al. 2011; Reis et al. 2012). Swift J1644+57 was initially discovered as a long-duration gamma-ray burst (GRB 110328A) by the *Swift* Burst Alert Telescope (BAT). *Swift* follow-up observations with the Ultraviolet and Optical Telescope (UVOT) and the X-ray Telescope (XRT) began 1475 s after the initial trigger. No source was seen in the UVOT observations, but a bright point source was found with the XRT (Bloom et al. 2011). It remained bright and highly variable for a long period, and retriggered the BAT three times. This high-energy transient is unlike any known events, such as active galactic nuclei (AGNs) or gamma-ray bursts (GRBs). The BAT and XRT spectral fits are consistent during the brightest flaring stage, and well fitted with a broken power-law model (Burrows et al. 2011). After considering the repeated extremely short time-scale X-ray flares, Wang & Cheng (2012) have proposed a later internal shock model for the X-ray flares of Swift J1644+57, in which the reverse shock is relativistic and the forward shock is Newtonian. From the strong emission lines of hydrogen and oxygen, the redshift of Swift J1644+57 is $z \sim 0.35$ (Levan et al. 2011). From the X-ray, optical, infrared and radio observations, it has been found that the position of this source is consistent with the nucleus of the host galaxy (Bloom et al. 2011). This event has not been detected by the *Fermi* Large Area Telescope (LAT) or by the Very Energetic Radiation Imaging Telescope Array System (VERITAS; Aliu et al. 2011). Only upper limits were given in the GeV and TeV bands.

The peak isotropic luminosity of Swift J1644+57 is about $\sim 2 \times 10^{48}$ erg s^{-1} (Bloom et al. 2011; Burrows et al. 2011), which is about 10^4 times larger than the Eddington luminosity of a 10^6-$M_\odot$ black hole. Because of this super-Eddington luminosity and the position of Swift J1644+57 relative to the centre of its host galaxy, it is suggested that Swift 1644+57 is powered by a relativistic jet created by accretion on to a 10^{6-7}-$M_\odot$ black hole (Bloom et al. 2011; Burrows et al. 2011; Shao et al. 2011). The jet Lorentz factor was limited to $\Gamma \leq 20$ from high-energy observations (Burrows et al. 2011), the event rate (Burrows et al. 2011) and radio observations (Zauderer et al. 2011; Berger et al. 2012). Wong, Huang & Cheng (2007) were the first to argue that the X-ray emission of a tidal disruption event might not necessarily come from the radiation of the accretion disc alone. Instead, it might be related to a jet. As the jet travels in the interstellar medium, a shock is produced and synchrotron radiation is expected. Wong et al. (2007) compared the light curve and the synchrotron radiation spectrum in their model with the observed data and found that the model provides a good explanation for the observed transient X-ray emission from NGC 5905 and the late-time spectrum. Some theoretical models have been proposed to explain the unusual features of this event. For example, Swift J1644+57 could be explained as a white dwarf disrupted by a 10^4-$M_\odot$ black hole (Krolik & Piran 2011) or as a tidal obliteration event, which disrupts a star in a deeply plunging

★E-mail: zouyc@hust.edu.cn (YCZ); fayinwang@nju.edu.cn (FYW); hrspksc@hku.hk (KSC)

orbit at periastron (Cannizzo, Troja & Lodato 2011). Lei & Zhang (2011) have suggested that the jet is launched by the Blandford–Znajek mechanism (Blandford & Znajek 1977) and have found that the spin parameter of the central black hole is very high. Furthermore, Lei, Zhang & Gao (2013) have inferred the inclination angle between the black hole spin axis and the star orbit. Saxton et al. (2012) have studied the X-ray timing and spectral evolution of this event and have found that the spectrum becomes mildly harder in its long-term evolution. Gao (2012) has argued that the outflow should be Poynting-flux-dominated. Using a two-dimensional simulation, De Colle et al. (2012) have shown that the stochastic contribution of the luminosity due to the feeding rate variability induced by instabilities can explain the X-ray light curve of Swift J1644+57. Berger et al. (2012) and Metzger, Giannios & Mimica (2012) have modelled the radio emission of Swift J1644+57 using the GRB afterglow model. Berger et al. (2012) have also found that the energy increase cannot be explained with continuous injection from an $L \propto t^{-5/3}$ tail and that the relativistic jet has a wide range of Lorentz factors. Most recently, Zauderer et al. (2013) have found that the X-ray flux has a sharp decline, by a factor of 170 at about 500 d.

Based on the late X-ray light curve, which is composed of multiple X-ray flares, we propose that the X-ray emission comes from the reverse shock produced by the late ejected shell colliding with the decelerating material, which is decelerated by the ambient medium through which it moves. The whole scenario of our model is as follows. At the beginning, the central engine ejects relativistic shells with higher velocity (corresponding to a higher Lorentz factor). They catch up with the outermost slower shell and the consequent reverse shocks produce the early (1–10^5 s) X-rays, as proposed by Wang & Cheng (2012). At later times, the central engine ejects shells with lower velocity (i.e. a lower Lorentz factor). At the same stage, the outermost shell has been decelerated by the medium, which drives an external shock. This external shock produces the radio emission (Berger et al. 2012; Metzger et al. 2012). Then, ejected shells collide with this outermost decelerating material, and the reverse shocks produce the late X-rays, which decreases with time as the density of the emitting region decreases. The late injection of the shells also enhances the total energy of the external shock, which provides the necessary energy resource to explain the late enhancement of the radio emission presented by Berger et al. (2012). In this paper, we mainly focus on the later emission of X-rays, which is produced by collisions between ejected shells and the decelerating material. We describe our model in Section 2, and we conclude in Section 3.

2 MODELLING

The X-ray emission shows very rapid flaring in the whole radiation period from the beginning until several 10^7 s. This suggests that the flares should not come from the continuous external shock. However, the external shock does exist, and might emit mainly at optical and radio frequencies when the early ejected shells combine and sweep the ambient medium.[1] With the continuous activity of the central engine fed by material still remaining around the central black hole, the late ejected shells will eventually catch up with the external decelerating shock, and a reverse shock will emerge back into the ejected shells. Berger et al. (2012) have also found that the outflow is structured and that the relativistic jet was produced with a wide range of Lorentz factors. Consequently, the forward shock will proceed into the shocked medium. However, if the number density of the shocked medium is high enough (corresponding to a weak non-relativistic forward shock, which depends on the contrast of the density between the two regions; Sari & Piran 1995), this forward shock will be weak enough and the corresponding emission would be negligible. Also, the bulk Lorentz factor of the reverse shock will be the same as that of the external shocked material. If the energy of the shell is much smaller than the kinetic energy of the external shock, the influence on the dynamics of the external shock can be neglected. The behaviour of the external shock can be described in the same way as a standard GRB afterglow (Sari, Piran & Narayan 1998).

The scenario for the late X-ray emission in our model is as follows. The continuous external shock mainly emits radio and optical emission, and the late ejected shells collide on the decelerating external shocked material. The reverse shock of each collision produces one flare of the X-ray emission. Superposition of all the flares by these episodically ejected shells composes the whole late-flaring X-ray light curve. The details of the scaling laws are as follows.

The Lorentz factor of the external shock is (Sari et al. 1998)

$$\gamma \simeq 4.3\, n_0^{-(1/8)}(1+z)^{3/8} E_{k,0,54}^{1/8} t_{\oplus,6}^{-(3/8)}, \quad (1)$$

where n is the number density of the medium, z is the redshift, $E_{k,0}$ is the isotropic kinetic energy of the external shock and $t_\oplus$ is the observer's time. The notation $Q = 10^x Q_x$ is used throughout the paper. The evolution of the Lorentz factor is consistent with the radio observation at 216 d after the BAT trigger (Berger et al. 2012). For example, at $t_\oplus = 216$ d, the Lorentz factor is about 2.2 for $E_{k,0} = 5 \times 10^{53}$ erg and $n = 0.2$ cm^{-3} from the observation. At the late time, the Lorentz factor γ has decreased into a relatively low region, and the edge of the jet will be seen by the observer for a normal jet opening angle $\theta_j = 0.1$. AGN jets are also confirmed from supermassive black holes. The apparent opening angle can be as high as tens of degrees in an AGN jet, while the intrinsic opening angle could be as low as a few degrees (Pushkarev et al. 2009). So, our choice of $\theta_j \sim 0.1$ is reasonable. For relativistic motion, the relation between the radius and observing time is $\mathrm{d}r = 2(1+z)\gamma^2 c\, \mathrm{d}t_\oplus$. Thus, the radius evolution with time is

$$r \simeq 2.71 \times 10^{18} n_0^{-(1/4)}(1+z)^{-(1/4)} E_{k,0,54}^{1/4} t_{\oplus,6}^{1/4}\ \mathrm{cm}. \quad (2)$$

We denote the reversely shocked and unshocked regions of the ejected shell as regions 3 and 4 ,respectively, and the forwardly shocked and unshocked medium as regions 2 and 1, respectively. The average Lorentz factor of protons in the reverse shock (region 3) is

$$\bar{\gamma}_3 \simeq \frac{1}{2}\left(\frac{\gamma_4}{\gamma_3} + \frac{\gamma_3}{\gamma_4}\right) \simeq \frac{\gamma_4}{2\gamma_3}$$

(if $\gamma_4 \gg \gamma_3$), where $\gamma_3 = \gamma$ is the bulk Lorentz factor of the reverse shock and γ_4 is the bulk Lorentz factor of the ejected shell. We obtain

$$\bar{\gamma}_3 \simeq 14.88 n_0^{1/8} \gamma_{4,2}(1+z)^{-(3/8)} E_{k,0,54}^{-(1/8)} t_{\oplus,6}^{3/8}. \quad (3)$$

Because of the spread of velocities inside a single shell, at times later than 10^6 s the spreading effect dominates the width of the ejected shell, which is $r/2\gamma_4^2$ (Sari & Piran 1995). The duration of

[1] Because the emission of the external shock very sensitively relies on the Lorentz factor (see Zou & Piran 2010 for more details), for the relatively low Lorentz factor of this tidally disruption event compared with that of a normal GRB, the flux density and the typical frequencies will be much lower than in GRBs.

the reverse shock is determined by the competition of the width of the shell and the jet angular size, that is,

$$\max\left(\frac{r}{2\gamma_4^2 c}, \frac{r\theta_j^2}{2c}\right) = \frac{r\theta_j^2}{2c},$$

because $\gamma_4 \sim 100$ and $\theta_j \sim 0.1$ in this case. Then, the duration of each pulse is

$$\delta T \simeq 4.5 \times 10^5 n_0^{-(1/4)} (1+z)^{3/4} \theta_{j,-1}^2 E_{k,0,54}^{1/4} t_{\oplus,6}^{1/4} \text{ s}. \quad (4)$$

This value of the duration is several times larger than the observed duration of the individual pulses. However, note that δT is very sensitive to the jet opening angle. It requires the value of θ_j to be slightly smaller than 0.1.

Similar to the treatment by Zou, Wu & Dai (2005), the number density of the reverse shock region is

$$n_3 = (4\bar{\gamma}_3 + 3) n_4 \simeq 1.8 \times 10^{-2} n_0^{5/8} \gamma_{4,2}^{-1} (1+z)^{9/8} \times E_{k,0,54}^{-(5/8)} E_{k,4,53} t_{\oplus,6}^{-(9/8)} \text{ cm}^{-3}, \quad (5)$$

where n_4 is the number density of the ejected shell, which is determined by the Lorentz factor γ_4 and the total kinetic energy $E_{k,4}$. The internal energy density of the reverse shock is

$$e_3 = \bar{\gamma}_3 n_3 m_p c^2 \simeq 4.0 \times 10^{-4} n_0^{3/4} (1+z)^{3/4} \times E_{k,0,54}^{-(3/4)} E_{k,4,53} t_{\oplus,6}^{-(3/4)} \text{ erg cm}^{-3}. \quad (6)$$

After the dynamical values are decided, we follow the method to obtain the synchrotron radiation of Sari et al. (1998). The electrons are accelerated into a power-law distribution: $N(\gamma_e) d\gamma_e = N_\gamma \gamma_e^{-p} d\gamma_e (\gamma_e > \gamma_m)$. Here, γ_e is the randomized electron Lorentz factor, γ_m is the minimum Lorentz factor of the accelerated electrons and p is the power-law index. Assuming that constant fractions ϵ_e and ϵ_B of the internal energy go into the electrons and the magnetic field, we have the magnetic field $B_3 = \sqrt{8\pi\epsilon_B e_3}$, where e_3 is the internal energy density of the shocked material. We obtain $\gamma_m = \epsilon_e(\bar{\gamma}_3 - 1)(m_p/m_e)(p-2)/(p-1)$, and $N_\gamma = n_3(p-1)\gamma_m^{p-1}$. The peak spectral power of the synchrotron emission for one electron is

$$P_{\nu,\max} = (1+z)\frac{\sigma_T m_e c^2 \gamma B_3}{3 q_e} \simeq 4.0 \times 10^{-23} n_0^{1/4} (1+z)^{7/4} E_{k,0,54}^{-(1/4)} E_{k,4,53}^{1/2} \times \varepsilon_{B,-1}^{1/2} t_{\oplus,6}^{-(3/4)} \text{ erg Hz}^{-1} \text{ s}^{-1}, \quad (7)$$

where σ_T is the Thomson cross-section and q_e is the electron charge. Thus, the peak observed flux density is

$$f_{\nu,\max} = (\gamma\theta_j)^2 \frac{N_e P_{\nu,\max}}{4\pi D^2} \simeq 4.8 \times 10^{-27} \gamma_{4,2}^{-1} D_{28}^{-2} (1+z)^{5/2} \theta_{j,-1}^2 E_{k,4,53}^{3/2} \times \varepsilon_{B,-1}^{1/2} t_{\oplus,6}^{-(3/2)} \text{ erg cm}^{-2} \text{ Hz}^{-1} \text{ s}^{-1}, \quad (8)$$

where $N_e = E_{k,4}/(\gamma_4 m_p c^2)$ is the total isotropic equivalent number of electrons in region 3 and D is the luminosity distance. Here, we need to consider the beaming factor $(\gamma\theta_j)^2 \simeq 0.11 n_0^{-(1/4)} (1+z)^{3/4} \theta_{j,-1}^2 E_{k,0,54}^{1/4} t_{\oplus,6}^{-(3/4)}$, because the jet opening angle is smaller than $1/\gamma$. Also, the isotropic solution should be corrected by the beaming factor (Rhoads 1999), while the lateral expansion is not considered for simplicity, a fact also supported by numerical simulations (Cannizzo, Gehrels & Vishniac 2004). With $z = 0.35$, the corresponding luminosity distance is $D \simeq 5.7 \times 10^{27}$ cm in a cosmological model $\Omega_M = 0.27$ and $\Omega_\Lambda = 0.73$ (Wright 2006).

The cooling Lorentz factor γ_c is defined such that the electron with γ_c approximately radiates all its kinetic energy in the dynamical time, that is, $(\gamma_c - 1) m_e c^2 = P(\gamma_c) t_{co}$, where $P(\gamma_e) = (4/3)\sigma_T c(\gamma_e^2 - 1)(B^2/8\pi)$ (Rybicki & Lightman 1979) is the synchrotron radiation power of an electron with Lorentz factor γ_e in the magnetic field B, and t_{co} is the dynamical time in the comoving frame. Then, the cooling Lorentz factor is $\gamma_c \simeq 6\pi m_e c \sigma_T B^2 t_{co}$, where $\sigma_T \simeq 6.65 \times 10^{-25}$ cm^2 is the Thompson scattering cross-section.

The typical frequency (in the observer's frame) for a given electron is $\nu_{syn} = 3(1+z)^{-1}\gamma\gamma_e^2 q_e B/(2\pi m_e c)$. The critical frequencies of the synchrotron emission are

$$\nu_m = 3(1+z)^{-1}\gamma\gamma_m^2 q_e B/(2\pi m_e c) \simeq 2.5 \times 10^{12} n_0^{1/2} \gamma_{4,2}^2 \varepsilon_{e,-(1/2)}^2 (1+z)^{-1} E_{k,0,54}^{-(1/2)} E_{k,4,53}^{1/2} \times \varepsilon_{B,-1}^{1/2} \text{ Hz}, \quad (9)$$

$$\nu_c = 3(1+z)^{-1}\gamma\gamma_c^2 q_e B/(2\pi m_e c) \simeq 7.7 \times 10^{16} n_0^{-(1/2)} (1+z)^{-2} \theta_{j,-1}^{-4} E_{k,0,54}^{1/2} E_{k,4,53}^{-(3/2)} \times \varepsilon_{B,-1}^{-(3/2)} t_{\oplus,6} \text{ Hz}. \quad (10)$$

The synchrotron self-absorbing frequency ν_a for $\nu_a < \nu_m < \nu_c$ is (Zou et al. 2005)

$$\nu_a = 1.1 \times 10^8 n_0^{1/5} \gamma_{4,2}^{-(8/5)} \varepsilon_{e,-(1/2)}^{-1} (1+z)^{(1/5)} E_{k,0,54}^{-(1/5)} \times E_{k,4,53}^{4/5} \varepsilon_{B,-1}^{1/5} t_{\oplus,6}^{-(6/5)} \text{ Hz}. \quad (11)$$

Sari et al. (1998) have given the formulae for the flux density in different spectral segments. The flux density of the late external reverse shock region $f_\nu(t_\oplus)$ (in units of erg cm^{-2} Hz^{-1} s^{-1}) for different segments are as follows:

$$f_\nu \simeq 1.37 \times 10^{-10} n_0^{-(1/2)} \gamma_{4,2} \nu_{17}^2 D_{28}^{-2} \varepsilon_{e,-(1/2)} (1+z)^{5/2} \times \theta_{j,-1}^2 E_{k,0,54}^{1/2} t_{\oplus,6}^{1/2}, \quad (12)$$

for $\nu < \nu_a < \nu_m < \nu_c$;

$$f_\nu \simeq 1.65 \times 10^{-25} n_0^{-(1/6)} \gamma_{4,2}^{-(5/3)} \nu_{17}^{1/3} D_{28}^{-2} \varepsilon_{e,-(1/2)}^{-(2/3)} \times (1+z)^{17/6} \theta_{j,-1}^2 E_{k,0,54}^{1/6} E_{k,4,53}^{4/3} \varepsilon_{B,-1}^{1/3} t_{\oplus,6}^{-(3/2)}, \quad (13)$$

for $\nu_a < \nu < \nu_m < \nu_c$;

$$f_\nu \simeq 8.28 \times 10^{-30} n_0^{3/10} \gamma_{4,2}^{1/5} \nu_{17}^{-(3/5)} D_{28}^{-2} \varepsilon_{e,-(1/2)}^{6/5} \times (1+z)^{19/10} \theta_{j,-1}^2 E_{k,0,54}^{-(3/10)} E_{k,4,53}^{9/5} \varepsilon_{B,-1}^{4/5} t_{\oplus,6}^{-(3/2)}, \quad (14)$$

for $\nu_a < \nu_m < \nu < \nu_c$;

$$f_\nu \simeq 7.26 \times 10^{-30} n_0^{1/20} \gamma_{4,2}^{1/5} \nu_{17}^{-(11/10)} D_{28}^{-2} \varepsilon_{e,-(1/2)}^{6/5} \times (1+z)^{9/10} E_{k,0,54}^{-(1/20)} E_{k,4,53}^{21/20} \varepsilon_{B,-1}^{1/20} t_{\oplus,6}^{-1}, \quad (15)$$

for $\nu_a < \nu_m < \nu_c < \nu$.

The X-rays observed by the XRT are in the range of 0.3–10 keV, corresponding to $\nu_1 = 7.2 \times 10^{16}$ Hz to $\nu_2 = 2.4 \times 10^{18}$ Hz. Equations (14) and (15) correspond to the X-rays. Because ν_m does not change with time. We find that ν_c was crossing the observed band by fitting the slope of the X-ray light curves (the trend of the peaks).

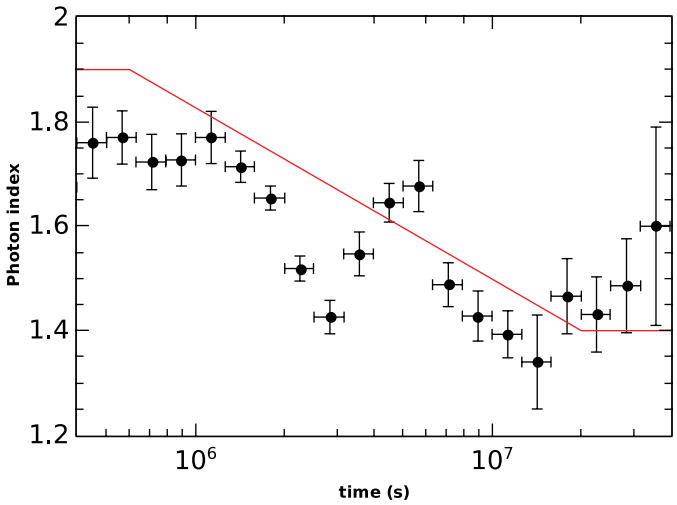

Figure 1. Photon index of Swift J1644+57 versus time. Data are taken from http://www.swift.ac.uk/xrt_spectra/00450158/. The solid line is the index from the model for the peak times, which roughly dominates the whole spectrum.

With a suitable tuning to model the observational light curves and the spectral evolution, we obtain a set of proper parameters, which are far from extreme: $p = 1.8$,[2] $n = 1$ cm^{-3}, $E_{k,4} = 3 \times 10^{53}$ erg, $E_{k,0} = 3 \times 10^{54}$ erg, $\varepsilon_B = 0.1$, $\varepsilon_e = 0.3$, $\gamma_4 = 70$ and $\theta_j = 0.05$. These parameters, including the Lorentz factor of the external shock γ, are consistent with the constraint from the radio observations. Berger et al. (2012) have found that the Lorentz factor of the external shock is $\gamma \sim 2.2$–6.0, that the ambient density is 0.2–60 cm^{-3} and that the jet energy is larger than 5×10^{53} erg using the radio observation up to 216 d after the BAT trigger. Metzger et al. (2012) have found that $\epsilon_e = 0.03$–0.1, that the ambient density is 1–10 cm^{-3} and that the opening angle is 0.01–0.1.

The scaling laws with time of the derived quantities are as follows. The Lorentz factor of the emitting region $\gamma \simeq 4.3 t_{\oplus,6}^{-(3/8)}$, which decreases with time, but might be slower than $t_{\oplus,6}^{-(3/8)}$ because new injected shells speed up the external shock slightly, which depends on the total energy of the late ejection. The duration of each pulse is $\delta T \simeq 1.9 \times 10^5 t_{\oplus,6}^{1/4}$ s, which is consistent with the duration of the pulse in the observed light curve. The slight widening with time has also been reported by Saxton et al. (2012). The characteristic frequency $\nu_m \simeq 8.1 \times 10^{11}$ Hz, which does not change with time and is always below the X-ray frequencies of the XRT. The cooling frequency $\nu_c \simeq 1.3 \times 10^{17}\, t_{\oplus,6}$ Hz divides the X-ray band in several epochs, for $t_\oplus < 6 \times 10^5$ s, $\nu_m < \nu_c < \nu_1 < \nu_2$, with X-ray spectral index $-(p/2)$ (i.e. -0.9), corresponding to the photon index 1.9. This value is larger than a rough average of the observed photon index 1.8. The reason for this is that ν_c is calculated for the time when the reverse shock just crosses the shell (ν_c decreases from the beginning until this time). Therefore, for each pulse, there is a period when ν_c is higher than the observed frequency and the case is $\nu_m < \nu < \nu_c$, and then the average photon index could be smaller than 1.9. For the time 6×10^5 s $< t_\oplus < 2 \times 10^7$ s, $\nu_m < \nu_1 < \nu_c < \nu_2$, with the X-ray spectral index between $[-(p/2), -(p-1/2)]$ [i.e. $(-0.9, -0.4)$], and for $t_\oplus > 2 \times 10^7$ s, $\nu_m < \nu_1 < \nu_2 < \nu_c$, with the X-ray spectral index $-[(p-1)/2]$ (i.e. -0.4). All the corresponding photon indices are shown in Fig. 1. The flux densities of synchrotron radiation in different ranges are $f_\nu \simeq 6.1 \times 10^{-28} t_{\oplus,6}^{-1}$ erg cm^{-2} Hz^{-1} s^{-1} for $\nu_m < \nu_c < \nu_1 < \nu_2$, which is suitable for time $t < 6 \times 10^5$ s. At $t = 6 \times 10^5$ s, $f_\nu \simeq 1.0 \times 10^{-27}$, and the flux is 4.0×10^{-10} erg cm^{-2} s^{-1}. This is consistent with the observation seen in Fig. 2. We find that $f_\nu \simeq 5.3 \times 10^{-28} t_{\oplus,6}^{-(3/2)}$ erg cm^{-2} Hz^{-1} s^{-1} for $\nu_m < \nu_1 < \nu_2 < \nu_c$, which is suitable for time $t > 2 \times 10^7$ s. Meanwhile, between (6×10^5 s, 2×10^7 s), the case is $\nu_m < \nu_1 < \nu_c < \nu_2$, and the flux should be contributed to by both bands. The temporal index should be between -1 and $-(3/2)$, and the photon index should be between 1.4 and 1.9 during this period, as shown in Fig. 1. We can clearly see the transition of the photon index from this figure, which can be understood clearly from the model (solid line). Although during the transitional period (6×10^5 s, 2×10^7 s) the photon indices vary with time and do not trace the solid line, this might result from the diversity of the late ejected shells. For times earlier than 6×10^5 s, the predicted flux is higher than the observed flux. This might be caused by the transition of the external shock from a coasting phase into a decelerating phase.

3 CONCLUSION AND DISCUSSION

In this paper, we have proposed a scenario for the late X-ray emission from Swift J1644+57 (i.e. a central engine produces long-lasting episodic relativistic ejecta). These ejecta catch up with the decelerating material, which sweeps the medium, and the reverse shock propagating back into the ejecta emits the observed flaring X-rays. Because the ejecta are shells but not a steady jet, the emission appears as flares. As shown in Figs 1 and 2, our model is consistent with the observed peaks of the flares on both the envelope of the light curve and the photon indices.

This scenario succeeds the 'prompt' emission picture proposed by Wang & Cheng (2012). Both scenarios are from the reversed shock of the central engine ejection, which gives a complete picture

[2] Note that because $p = 1.8 < 2$, a cut-off Lorentz factor of the shock electrons γ_{max} should be introduced to make the model self-consistent, and this might change γ_m slightly (Dai & Cheng 2001). However, the value of γ_{max} depends on different models (Bhattacharya 2001; Dai & Cheng 2001), and the introduction of γ_{max} into γ_m will make the expressions much more complicated. To keep the simplicity, we have chosen not to take this γ_{max} effect into account.

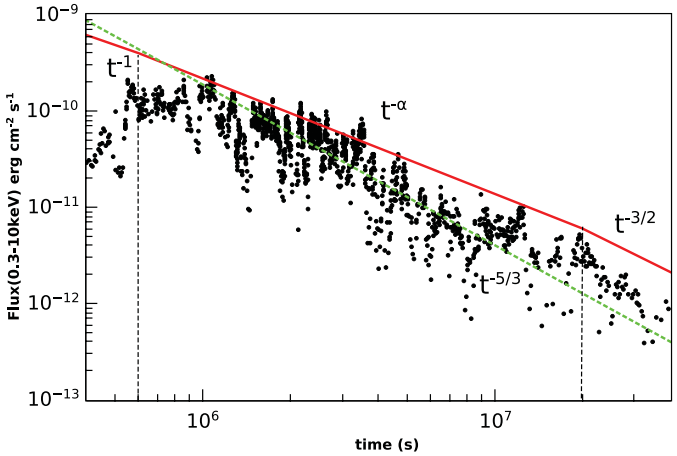

Figure 2. X-ray light curve of Swift J1644+57. Data are taken from http://www.swift.ac.uk/xrt_curves/00450158/ (Evans et al. 2009). The solid three-segment line is the envelope for the peaks from the model. The vertical dashed lines indicate the time for the change of time behaviour because of the frequency crossing. Here, α varies with time from 1 to 1.5. The dotted line is a $t^{-5/3}$ slope, shown for comparison.

for this event. At the beginning, the central engine produces shells with higher velocity. They catch up with the outermost slower shell and the consequent reverse shocks produce the early (1–10^5 s) X-rays. At later times, the central engine ejects shells with relatively lower velocity (assumed to be with the same Lorentz factor γ_4 for the whole late times). At the same stage, the outermost shell has been decelerated by the medium, which drives an external shock. Then, ejected shells collide with this decelerating material, and the reverse shocks produce the late X-rays, which decrease with time. The late injection of the shells also enhances the total energy of the external shock, which provides the necessary energy resource to explain the late enhancement of the radio emission. Our model predicts that the X-ray peaks will continue their $t^{-1.5}$ slope until the external shock dominates the radiation, which will appear shallower with a less variable light curve. This can be examined using follow-up observations.

Although the scenario for late X-rays is a follow-up to the scenario for earlier X-ray emission proposed by Wang & Cheng (2012), there are some significant differences. First, the objective is different. Wang & Cheng (2012) treated the early emission, while in this paper we treat the late X-ray emission with obvious flares. Secondly, the scenario is different. Here, the reverse shock is produced by collisions between later ejected shells and decelerating material. However, the reverse shock in Wang & Cheng (2012) is produced by two shells colliding. The physical origin of the reverse shock is quite different. Thirdly, in this paper, the width of the reversely shocked region 3 is much longer than that of Wang & Cheng (2012), because of the spreading of shells. So, the duration of the reverse shock is also long. The duration of the X-ray pulse is found to be about 10^5 s from observations (Saxton et al. 2012), which is consistent with our model (see equation 4). In our model, as the relativistic jet shuts off, there is no shell to catch up with the decelerating material, and the emission of the reverse shock (mainly in X-rays) disappears. The X-ray emission of the external shock is weak, which is consistent with *Swift* and *Chandra* observations (Zauderer et al. 2013).

The origin of the hard electron distribution ($p < 2$) is not yet clear. The observations have also confirmed the evidence for a hard electron distribution in some GRBs (Dai & Cheng 2001; Huang, Cheng & Gao 2006; Covino et al. 2010). Simulations of the *Fermi* process in relativistic shocks, including large angle scattering, have resulted in hard electron energy spectra (Stecker, Baring & Summerlin 2007).

The synchrotron self-Compton (SSC) scattering is not considered here, because the Compton parameter Y is much less than 1. Without including Klein–Nishina effects, $Y_{\rm noKN} \simeq (-1+\sqrt{1+4\epsilon_{\rm rad}\epsilon_{\rm e}/\epsilon_B})/2$ (Sari & Esin 2001), the radiation efficiencies are $\epsilon_{\rm rad} = (\gamma_{\rm c}/\gamma_{\rm m})^{2-p}$ (only suitable for $p > 2$, however) for $\gamma_{\rm c} > \gamma_{\rm m}$ and $\epsilon_{\rm rad} = 1$ for $\gamma_{\rm c} < \gamma_{\rm m}$. For the parameters chosen here, $Y_{\rm noKN} \simeq 7$. However, for the typical Lorentz factor $\gamma_{\rm c} \simeq 5\times10^6 t_{\oplus,6}^{7/8}$, and the typical frequency in the comoving frame $\nu'_{\rm c} \sim 10^{18} t_{\oplus,6}^{5/8}$ Hz, the main SSC emission at $\sim 2\gamma_{\rm c}^2\nu_{\rm c}$ (Sari & Esin 2001) is deeply suppressed by the Klein–Nishina effects and the final Y parameter is much less than 1. This is also consistent with non-detection by *Fermi* and the High Energy Stereoscopic System (HESS) at higher energy bands.

Our model can also be used for GRBs with long-term X-ray flares, such as GRB 070311 (Vergani & Guidorzi 2008) and GRB 071118 (Cummings et al. 2007). The off-axis case of our model can also be applied to the Galactic Centre, where a gas cloud is ongoing to the central black hole (Gillessen et al. 2012). If this accretion were also to produce episodic jets, the jets would most likely not point to Earth (i.e. the off-axis case).

ACKNOWLEDGEMENTS

We are grateful to Xuefeng Wu and Weihua Lei for discussing the paper with us. We thank an anonymous referee for helpful comments and suggestions. We thank Kevin MacKeown for a critical reading of the manuscript. This work made use of data supplied by the UK *Swift* Science Data Centre at the University of Leicester. This work was supported by the National Basic Research Program of China (973 Program, Grant No. 2014CB845800). KSC is supported by a GRF grant from the Hong Kong Government under HKU 701013. FYW and YCZ are supported by the National Natural Science Foundation of China (grants 11103007, 11033002 and U1231101).

REFERENCES

Aliu E. et al., 2011, ApJ, 738, L30
Ayal S., Livio M., Piran T., 2000, ApJ, 545, 772
Berger E., Zauderer A., Pooley G. G., Soderberg A. M., Sari R., Brunthaler A., Bietenholz M. F., 2012, ApJ, 748, 36
Bhattacharya D., 2001, Bull. Astron. Soc. India, 29, 107
Blandford R. D., Znajek R. L., 1977, MNRAS, 179, 433

Bloom J. S. et al., 2011, Sci, 333, 203
Burrows D. N. et al., 2011, Nat, 476, 421
Cannizzo J. K., Gehrels N., Vishniac E. T., 2004, ApJ, 601, 380
Cannizzo J. K., Troja E., Lodato G., 2011, ApJ, 742, 32
Covino S. et al., 2010, A&A, 521, A53
Cummings J. R. et al., 2007, GCN Circ., 7106, 1
Dai Z. G., Cheng K. S., 2001, ApJ, 558, L109
De Colle F., Guillochon J., Naiman J., Ramirez-Ruiz E., 2012, ApJ, 760, 103
Evans P. A. et al., 2009, MNRAS, 397, 1177
Gao W. H., 2012, ApJ, 761, 113
Gillessen S. et al., 2012, Nat, 481, 51
Hills J. G., 1975, Nat, 254, 295
Huang Y. F., Cheng K. S., Gao T. T., 2006, ApJ, 637, 873
Krolik J. H., Piran T., 2011, ApJ, 743, 134
Lacy J. H., Townes C. H., Hollenbach D. J., 1982, ApJ, 262, 120
Lei W. H., Zhang B., 2011, ApJ, 740, L27
Lei W. H., Zhang B., Gao H., 2013, ApJ, 762, 98
Levan A. J. et al., 2011, Sci, 333, 199
Metzger B. D., Giannios D., Mimica P., 2012, MNRAS, 420, 3528
Pushkarev A. B., Kovalev Y. Y., Lister M. L., Savolainen T., 2009, A&A, 507, L33
Rees M. J., 1988, Nat, 333, 523
Reis R. C., Miller J. M., Reynolds M. T., Gültekin K., Maitra D., King A. L., Strohmayer T. E., 2012, Sci, 337, 949
Rhoads J. E., 1999, ApJ, 525, 737
Rybicki G. B., Lightman A. P., 1979, Radiative Processes in Astrophysics. Wiley, New York
Sari R., Esin A. A., 2001, ApJ, 548, 787
Sari R., Piran T., 1995, ApJ, 455, L143
Sari R., Piran T., Narayan R., 1998, ApJ, 497, L17
Saxton C. J., Soria R., Wu K., Kuin N. P. M., 2012, MNRAS, 422, 1625
Shao L., Zhang F-W., Fan Y-Z., Wei D-M., 2011, ApJ, 734, L33
Stecker F. W., Baring M. G., Summerlin E. J., 2007, ApJ, 667, L29
Strubbe L. E., Quataert E., 2009, MNRAS, 400, 2070
Strubbe L. E., Quataert E., 2011, MNRAS, 415, 168
Ulmer A., 1999, ApJ, 514, 180
Vergani S. D., Guidorzi C., 2008, Int. J. Mod. Phys. D, 17, 1359
Wang F. Y., Cheng K. S., 2012, MNRAS, 421, 908
Wong A. Y. L., Huang Y. F., Cheng K. S., 2007, A&A, 472, 93
Wright E. L., 2006, PASP, 118, 1711
Zauderer B. A. et al., 2011, Nat, 476, 425
Zauderer B. A., Berger E., Margutti R., Pooley G. G., Sari R., Soderberg A. M., Brunthaler A., Bietenholz M. F., 2013, ApJ, 767, 152
Zou Y. C., Piran T., 2010, MNRAS, 402, 1854
Zou Y. C., Wu X. F., Dai Z. G., 2005, MNRAS, 363, 93

This paper has been typeset from a TEX/LATEX file prepared by the author.